Adsorption of Ascorbic Acid on the C_{60} Fullerene

S. G. Santos, J. V. Santana, F. F. Maia, Jr., V. Lemos, and V. N. Freire

Departamento de Física, Universidade Federal do Ceará, Campus do Pici Caixa Postal 6030, 60455-900 Fortaleza, Ceará, Brazil

E. W. S. Caetano*

Centro Federal de Educaçao Tecnológica do Ceará, Av. 13 de Maio, 2081 Benfica, 60040-531 Fortaleza, Ceará, Brazil

B. S. Cavada

Departamento de Bioquímica, Laboratório de Bioquímica Molecular, Universidade Federal do Ceará, Campus do Pici, 60455-900 Fortaleza, Ceará, Brazil

E. L. Albuquerque

Departamento de Física Teórica e Experimental, Universidade Federal do Rio Grande do Norte, 59072-900 Natal, Rio Grande do Norte, Brazil

Received: June 01, 2008; Revised Manuscript Received: August 15, 2008

Adsorption of ascorbic acid (AsA) on C_{60} is investigated using classical molecular mechanics and density functional theory (DFT). Classical annealing was performed to explore the space of molecular configurations of ascorbic acid adsorbed on C_{60}, searching for optimal geometries. From the structure with the smallest total energy, 10 initial configurations were prepared by applying rotations of 90° about three orthogonal axes. Each one of these configurations was optimized using DFT (for both LDA and GGA exchange−correlation functionals), and an estimate of their total and adsorption energies was found. Different configurations have minimal adsorption energies (defined here as the total energy of the adsorbate minus the total energy of the separate molecules) from −0.54 to −0.10 eV, with distinct optimal distances between the AsA and C_{60} centers of mass. According to a Hirshfeld population analysis, AsA is, in general, an acceptor of electrons from C_{60}. Our results demonstrate the feasibility of noncovalent functionalization of C_{60} with AsA and provide minimal energy values for the several different configurations investigated. These results should be considered in reactions as a possible way to prevent against the oxidative damage and toxicity of C_{60}. The beneficial effects of using AsA−C_{60} includes its action when administered together with levodopa, against the neurotoxicity generated by levodopa isolated, which opens new strategies for the Parkinson's disease treatment.

I. Introduction

Following the buckminsterfullerene C_{60} discovery,[1,2] it was soon acknowledged that its poor solubility in polar solvents (which has implications in the formation of aggregates in aqueous solutions) is detrimental for biological applications. To circumvent this difficulty, several routes to attach chemical groups to C_{60} have been proposed,[3,4] leading to a wide variety of derivatives with distinct physical and chemical properties. Numerous experiments have established prospective applications for C_{60} derivatives in many fields such as enzymatic inhibition, anti-HIV activity, neuroprotection, antibacterial, DNA cleavage, and photodynamic therapy.[5] Photodynamic therapy with fullerenes either pristine or functionalized with various solubilizing groups was recently reviewed, outlining the viability of several applications.[6] It is the functional group that makes the fullerene-derivatized soluble and therefore able to interact with biological systems.

The functionalization of fullerenes is achieved through covalent bonding or physical interaction of foreign species. It has been demonstrated that the covalent bonding of amino acids, hydroxyl and carboxyl groups, and so forth through the replacement of some of the C═C double bonds improves the C_{60} ability to interact with the biological environment.[7] An alternative nondestructive method for solubilization is based on noncovalent binding, as observed for carbon nanotube solubilization in organic compounds for which the weaker binding ability is described in terms of van der Waals interactions.[8] Although many prospective applications for fullerene-soluble complexes exist, their cytotoxicity effects on living cells should be brought into balance.

As the cytotoxicity is a sensitive function of surface derivatization,[9−11] the existence of a wide range of biologically compatible solvents improves the versatility of functionalization, thereby minimizing cytotoxicity effects. In this aspect, ascorbic acid (AsA) is timely; with the chemical formula $C_6H_8O_6$, whose L-enantiomer is popularly known as vitamin C, it is an organic acid with antioxidant properties. In addition, it has an essential role as an enzymatic cofactor for the synthesis of biologically important molecules such as collagen, carnithine, catecholamine, myelin, and neuroendocrine peptides.[12,13] AsA is absolutely essential for human existence,[14] but it is not synthesized by

* To whom correspondence should be addressed.

10.1021/jp8048263 CCC: $40.75
Published on Web 10/22/2008

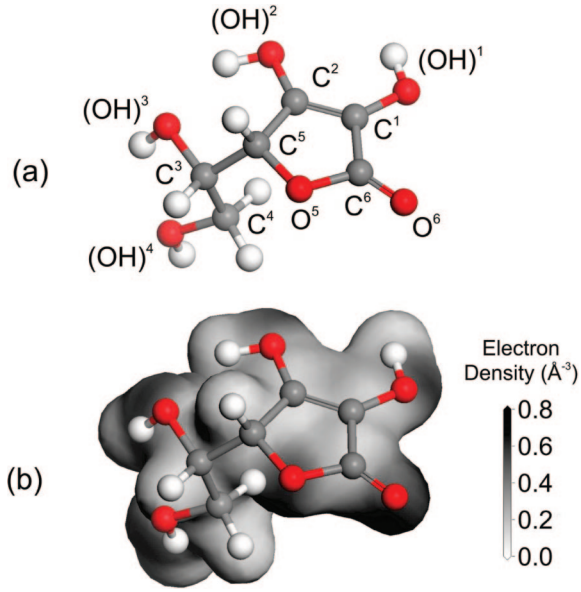

Figure 1. (a) Ascorbic acid ($C_6H_8O_6$) molecule with atom labels used in this work; (b) electron density projected onto an electrostatic potential isosurface.

human cells. It has been shown that the combination of this antioxidant with C_{60} completely prevents the oxidative damage and resultant toxicity of nano-C_{60} (sparingly underivatized fullerene colloids).[15] Moreover the C_{60}−ascorbic acid complex was found to protect cultured chromaffin cells against levodopa toxicity,[16] thus suggesting the beneficial use of AsA−C_{60}, associating it with levodopa, as an efficient treatment of Parkinson's disease.[16] It is also believed that AsA−C_{60} should be more effective in preventing oxidative damage than C_{60} alone, both being potent antioxidants. Consequently, focus on a detailed picture of the AsA bonding to C_{60} is of fundamental importance for biological applications of AsA -functionalized C_{60}. Whether AsA can bind covalently or not to C_{60} has yet to be demonstrated, prior to considering water effects.

The purpose of this work is to give a complete description of ascorbic acid interaction with buckminsterfullerene, including the effect of different spatial orientations of AsA relative to the C_{60} molecule. With the help of classical molecular dynamics, the best molecular geometry corresponding to the strongest binding of AsA adsorbed on C_{60} was found. Molecular dynamics simulations are the most indicated computer program for systems involving a large number of atoms. The alternative ab initio methods in such cases require much more computational time, making the task impossible in several cases. Therefore, for reasons of computational economy, we ran our first-principles simulations using the classically optimized geometries. Quantum ab initio density functional theory (DFT) simulations, in both the local density and generalized gradient approximations, LDA[17] and GGA,[18] respectively, were carried out to estimate the AsA−C_{60} binding energy. Afterward, the electron transfer between the AsA and C_{60} molecules was calculated to assess the noncovalent nature of their interaction.[19]

II. Computational Details and Classical Calculations Results

As depicted in Figure 1a, the ascorbic acid molecule is relatively small, with four −OH and two −CO groups that confer its antioxidant characteristics. Nine stable AsA structures were found experimentally in AsA crystals at low temperature,[20] while full optimizations for 36 AsA conformers have been

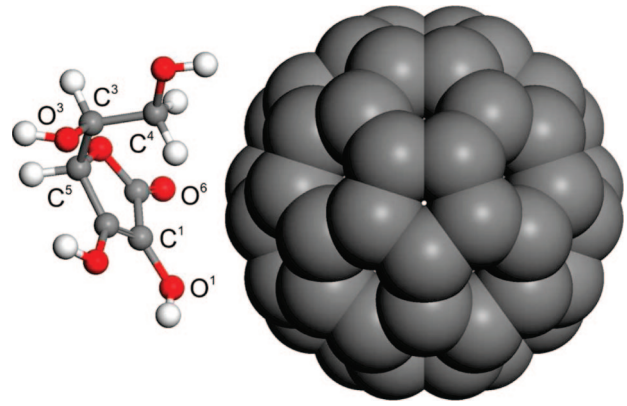

Figure 2. Atomic configuration with the lowest total energy for the AsA molecule adsorbed on C_{60} obtained after classical annealing and geometry optimization. O^1, O^6, C^1, and C^4 are the non-hydrogen atoms with the smallest distances relative to the C_{60} center of mass. O^3, C^3, and C^5 are the farthest ones.

reported through ab initio calculations using different theory levels and basis sets, RHF/6-31G, RHF/6-31G(d,p), RHF/6-311+G(d,p), and MP2/6-31(d,p).[21] The conformations of protonated and deprotonated AsA, as well as that of oxidized AsA, were studied recently.[22,23] Figure 1b shows the calculated electron density projection onto an electrostatic potential iso surface of a possible conformation of isolated AsA. As expected, oxygen atoms present the highest electron density (darker regions) due to their stronger electronegativity in comparison with carbon and hydrogen.

In order to find the best geometry for the AsA−C_{60} adsorption, a classical annealing simulation was carried out using the Forcite Plus code. The Universal force field was adopted to perform this simulation. The cutoff radius was chosen to be 18.5 Å. We carried out the annealing as follows; a total of 100 annealing cycles was simulated with an initial (midcycle) temperature of 200 K (300 K) and 50 heating ramps per cycle, with 100 dynamic steps per ramp. Using the NVT ensemble, we performed the molecular dynamics with a time step of 1 fs and a Nosé thermostat. After each cycle, the smallest energy configuration was optimized. Only the atoms of the AsA molecule were allowed to move during the calculations, the C_{60} atomic positions being kept fixed.

The best geometry that we found after the annealing/geometry optimization procedure is shown in Figure 2. The non-hydrogen atoms belonging to the AsA molecule closest to the C_{60} center of mass are O^1 (6.37 Å), C^4 (6.74 Å), C^1 (6.80 Å), and O^6 (6.85 Å). The two hydrogen atoms bound to the C^4 atom have the smallest distances to the C_{60} center of mass, 6.13 and 6.31 Å, followed by H^4 (6.41 Å) and H^1 (6.58 Å). On the other hand, the O^3, C^5, C^3, and O^5 are the farthest ones, with distances of 8.77, 8.17, 8.08, and 7.88 Å, respectively. To obtain the distance between a given atom and the approximately spherical surface of C_{60}, we should subtract 3.56 Å (the distance between any carbon atom belonging to the simulated C_{60} and the molecular center of mass).

Using the configuration of Figure 2, namely, $\Gamma_{(0,0,0)}$, we have built a set of inputs for a quantum first-principles geometry optimization. These inputs were generated by rotating the classically optimized $\Gamma_{(0,0,0)}$ AsA molecule about three arbitrary orthogonal axes (labeled x, y, and z), passing through its center of mass, and keeping the C_{60} atoms fixed. Only rotations of 90° about each axis were allowed. For example, the configuration obtained by rotating the molecule by 90° around the x axis was labeled $\Gamma_{(90,0,0)}$. Only 10 inputs were chosen through

this method, $\Gamma_{(0,0,0)}$, $\Gamma_{(90,0,0)}$, $\Gamma_{(180,0,0)}$, $\Gamma_{(270,0,0)}$, $\Gamma_{(0,90,0)}$, $\Gamma_{(0,180,0)}$, $\Gamma_{(0,270,0)}$, $\Gamma_{(0,0,90)}$, $\Gamma_{(0,0,180)}$, and $\Gamma_{(0,0,270)}$. We have considered these as a representative sampling of the space of initial configurations to investigate the trends of AsA adsorption on C_{60} using the quantum ab initio approach.

All quantum calculations were carried out using the DMOL3 code[24] in the density functional theory (DFT) framework. Core and valence electrons were considered explicitly, and a double numerical basis set (DNP) was chosen to expand the electronic eigenstates with an orbital cutoff radius of 3.7 Å. The exchange−correlation potential was considered in both the local density and generalized gradient approximations, LDA and GGA, respectively. The LDA exchange−correlation functional is the one parametrized by Perdew and Wang;[17] in the GGA approach, the Perdew−Burke−Ernzerhof[18] exchange−correlation functional was adopted. To study the interaction between AsA and C_{60}, we let the geometry of the isolated AsA molecule relax up to a total energy minimum to be attained.

III. Features of the Adsorption

The results of the first-principles optimizations are shown in Figures 3 and 4 and are also available as.mol files for download; see Supporting Information available at http://www.placesite-here.com. On the left side of each figure, it is possible to check the final molecular geometries obtained after the LDA simulations. GGA results have qualitatively the same general features of the LDA approach, differing only by the interatomic and intermolecular distances, tending to underestimate the strength of covalent and noncovalent bonds, leading to larger lengths in comparison to LDA. In order to give a more quantitative view of the optimized geometries, we have plotted a distance profile for each conformation of AsA adsorbed on C_{60}. The plots take into account only the non-hydrogen atoms (carbon and oxygen) of the AsA molecule, displaying their distances to the C_{60} center of mass and revealing the most relevant details of the atomic geometries of each AsA adsorbate. The distance between a given atom (A) and the C_{60} center of mass (CM) is denoted by d(A−CM), and the distance between the AsA and C_{60} CMs is d(CM−CM).

The total energy for all AsA−C_{60} configurations is presented in Table 1. The structure optimized from the geometry with minimal total energy after the classical annealing, $\Gamma_{(0,0,0)}$, has the smallest total energy also in both LDA and GGA first-principles calculations (for simplicity, we will use here the same Γ indexes to label structures from both classical and quantum results). The other geometries, however, have total energies very close to the $\Gamma_{(0,0,0)}$ case, being larger in comparison by 0.74 eV (0.49 eV) at most for $\Gamma_{(0,270,0)}$ if the LDA (GGA) exchange−correlation functional is used. LDA total energies for the other Γ adsorbates relative to $\Gamma_{(0,0,0)}$ show a variation larger than that observed for the GGA ones, from 0.42 to 0.74 eV (in contrast, GGA results vary from 0.42 to 0.49 eV). It is known that for various systems, like hydrogen-bonded complexes, some of van der Waals type and others with strong dipole−dipole character, using the local density approximation leads to better results in comparison to the GGA approximation. In these types of systems, introducing a dependence on the electron density derivatives leads to worse interaction energies.[25] In fact, it was shown that the LDA approach describes well the distance between the layers of graphite,[26,27] rare-gas atoms adsorbed on graphite surfaces,[28,29] the intermolecular distance in a face-centered cubic crystal of C_{60},[30,31] and the intermolecular interaction potentials of the methane dimer.[32] It is reasonable, we believe, to assume that DFT-LDA calculations can describe nonbonding interactions

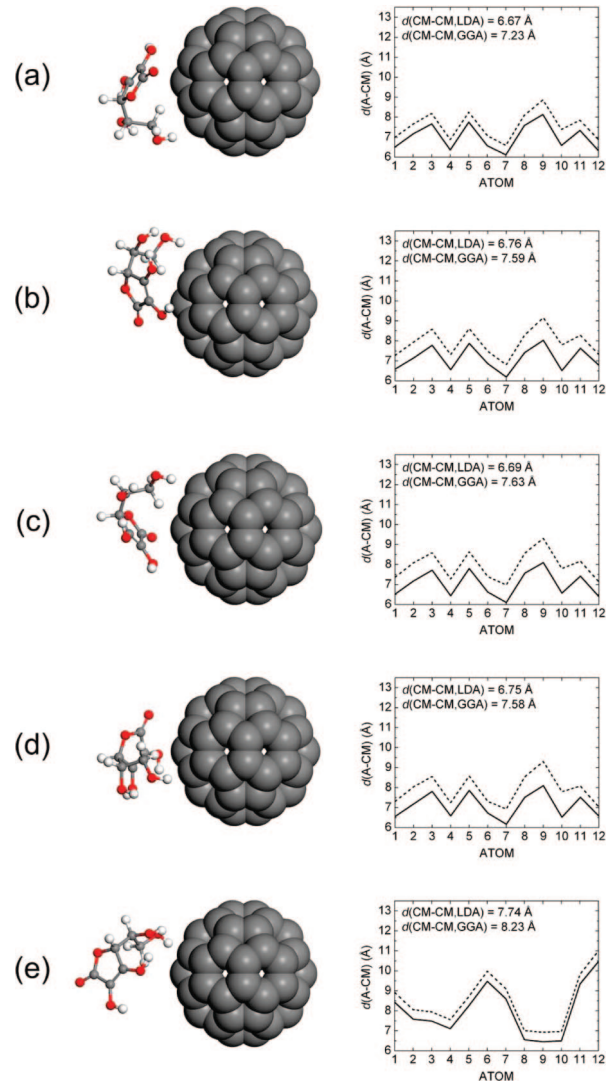

Figure 3. Left: LDA-optimized geometries obtained from the $\Gamma_{(0,0,0)}$ (a), $\Gamma_{(90,0,0)}$ (b), $\Gamma_{(180,0,0)}$ (c), $\Gamma_{(270,0,0)}$ (d), and $\Gamma_{(0,90,0)}$ (e) initial configurations. Right: Atomic distances d(A−CM) to the C_{60} center of mass (CM) for each geometry obtained in the LDA (solid lines) and GGA (dashed lines) approximations. Atoms 1−6 (7−12) correspond to C^1−C^6 (O^1−O^6). The d(CM−CM) is the distance between the AsA and C_{60} CMs.

in carbon systems such as AsA−C_{60} as well. Thus, the focus of our attention was mainly directed to the computationally less expensive LDA results, using the GGA data only to check for structural differences between the geometries predicted from both methods. In systems with strong charge-transfer effects (not the system studied in this work, as our population analysis indicates), however, the introduction of contributions from electron density derivatives in the exchange−correlation functional improves the accuracy.

The lowest-energy geometry, $\Gamma_{(0,0,0)}$, for both LDA and GGA calculations is qualitatively similar to the original classically optimized geometry, with the same pattern of atomic distances from the C_{60} center of mass, C^1, C^4, O^1, and O^6 being the nearest, and C^3, C^5, O^3, and O^5 being the farthest atoms (see Figure 3a). As stated before, the GGA data follow very closely the LDA curves in general, with the most pronounced difference observed for the $\Gamma_{(0,0,90)}$ (Figure 4c) followed by the $\Gamma_{(0,270,0)}$ (Figure 4b) structure. The second lowest LDA total energy conformation, $\Gamma_{(0,0,180)}$ (Figure 4d), has C^3, C^5, O^3, and O^5 closest to the C_{60} center of mass and C^1, C^4, O^1, and O^6 as the

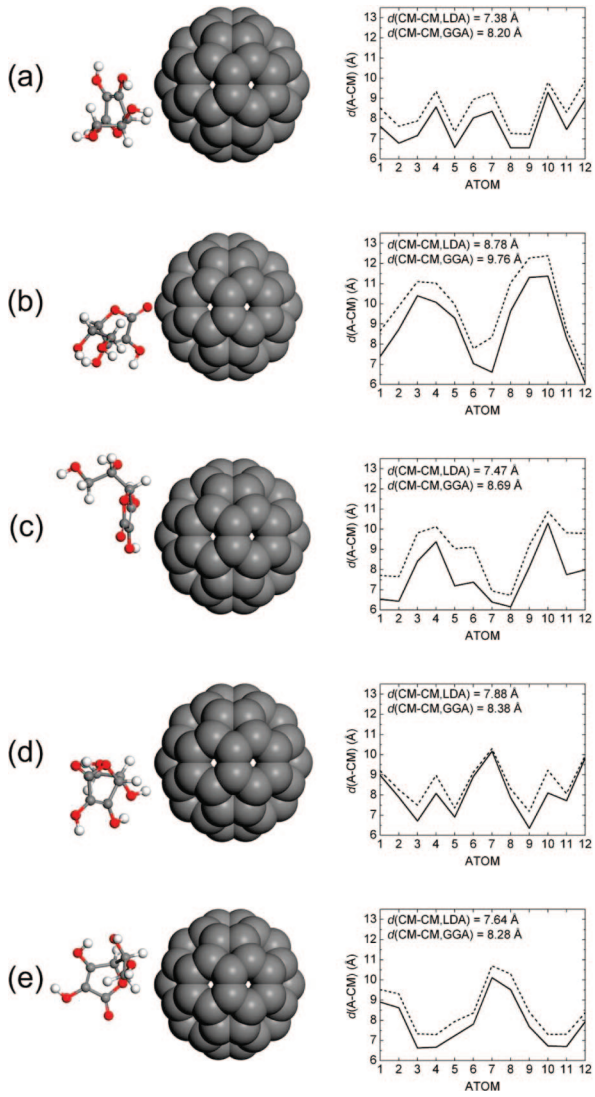

Figure 4. Left: LDA-optimized geometries obtained from the $\Gamma_{(0,180,0)}$ (a), $\Gamma_{(0,270,0)}$ (b), $\Gamma_{(0,0,90)}$ (c), $\Gamma_{(0,0,180)}$ (d), and $\Gamma_{(0,0,270)}$ (e) initial configurations. Right: Atomic distances d(A−CM) to the C_{60} center of mass for each geometry obtained in the LDA (solid lines) and GGA (dashed lines) approximations. Atoms 1−6 (7−12) correspond to C^1−C^6 (O^1−O^6). The d(CM−CM) is the distance between the AsA and C_{60} CMs.

TABLE 1: Total Energy of the AsA−C_{60} Adsorbates Optimized Using the LDA and GGA Exchange−Correlation Functionals[a]

starting geometry	total energy (eV)	
	LDA	GGA
$\Gamma_{(0,0,0)}$	−80145.7	−80746.3
	total energy relative to the $\Gamma_{(0,0,0)}$ (eV)	
	LDA	GGA
$\Gamma_{(90,0,0)}$	+0.52	+0.44
$\Gamma_{(180,0,0)}$	+0.45	+0.44
$\Gamma_{(270,0,0)}$	+0.52	+0.43
$\Gamma_{(0,90,0)}$	+0.70	+0.45
$\Gamma_{(0,180,0)}$	+0.88	+0.48
$\Gamma_{(0,270,0)}$	+0.74	+0.49
$\Gamma_{(0,0,90)}$	+0.67	+0.44
$\Gamma_{(0,0,180)}$	+0.42	+0.48
$\Gamma_{(0,0,270)}$	+0.72	+0.42

[a] The respective initial geometries, as obtained from classical annealing, are indicated.

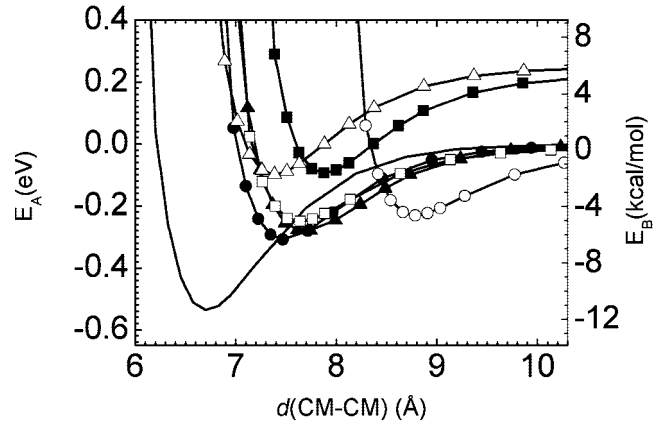

Figure 5. LDA adsorption energy of AsA on C_{60} as a function of d(CM−CM) for the geometries optimized from $\Gamma_{(0,0,0)}$ (solid line only), $\Gamma_{(0,0,180)}$ (solid squares), $\Gamma_{(0,0,90)}$ (solid circles), $\Gamma_{(0,90,0)}$ (solid triangles), $\Gamma_{(0,0,270)}$ (open squares), $\Gamma_{(0,270,0)}$ (open circles), $\Gamma_{(0,180,0)}$ (open triangles).

outermost. The d(CM−CM) is maximum for the $\Gamma_{(0,270,0)}$ configuration, 8.78 (LDA) and 9.76 Å (GGA). The smallest values of d(CM−CM), on the other hand, are observed for Γ,: 6.67 (LDA) and 7.23 Å GGA. It can be seen that $\Gamma_{(0,0,0)}$, $\Gamma_{(90,0,0)}$, $\Gamma_{(180,0,0)}$, and $\Gamma_{(270,0,0)}$ resemble one another very closely (Figure 3a−d). For the other Γ geometries, no similarities were found.

Looking now to the strength of the AsA−C_{60} interaction, we define the adsorption energy E_A as

$$E_A = E(\mathrm{AsA} + C_{60}) - E(C_{60}) - E(\mathrm{AsA}) \qquad (1)$$

where $E(C_{60})$ is the total energy for the isolated C_{60}, E(AsA) is the total energy of the AsA molecule, and E(AsA + C_{60}) is the total energy for the AsA−C_{60} geometry. The basis set superposition error was neglected by us due to the high quality of the basis set chosen.[33] The LDA adsorption energy for each optimized structure was investigated by translating the AsA atoms (with no change of molecular geometry) along lines parallel to the axis formed by joining the AsA and C_{60} CMs, thus changing d(CM−CM). The LDA adsorption energies are presented in Figure 5. Some caution must be exerted in analyzing E_A for each case due to the trend of overbinding observed in the local density approximation of the exchange−correlation functional. One can see that the $\Gamma_{(0,0,0)}$ geometry, again, has the smaller minimum at −0.54 eV in comparison with the other Γ structures, corresponding to the strongest binding. The results for the $\Gamma_{(90,0,0)}$, $\Gamma_{(180,0,0)}$, and $\Gamma_{(270,0,0)}$ are not shown in the figure due to their structural similarity with $\Gamma_{(0,0,0)}$. The second lowest value of E_A is observed for the $\Gamma_{(0,0,90)}$ structure, −0.31 eV, followed by $\Gamma_{(90,0,0)}$ (−0.28 eV), $\Gamma_{(0,90,0)}$ (−0.25 eV), $\Gamma_{(0,0,180)}$ (−0.23 eV), $\Gamma_{(0,180,0)}$ (−0.10 eV), and $\Gamma_{(0,270,0)}$ (−0.10) eV. It can be noted that E_A does not have the same ordered minimal energy configuration as that observed for the total energy, $E(\Gamma_{(0,0,0)}) < E(\Gamma_{(0,270,0)}) < E(\Gamma_{(0,0,270)}) < E(\Gamma_{(0,0,90)}) < E(\Gamma_{(90,0,0)}) < E(\Gamma_{(0,0,180)}) < E(\Gamma_{(0,180,0)})$.

Finally, the charge transfer between the AsA and C_{60} molecules was estimated by using the traditional Mulliken population analysis (MPA),[34] as well as the Hirshfeld population analysis (HPA)[35] and an electrostatic fitting of electric charges.[36] The first method has some problems attributed mainly to the arbitrary division of the overlap population. In cases where the electron transfer tends to zero, Fukui function indices obtained using MPA are unpredictable.[37] Hirshfeld charge assignment,

TABLE 2: AsA Population Analysis from LDA Data for Each Adsorption Configuration

starting geometry	AsA electric charge (e)		
	Mulliken	Hirshfeld	ESP
$\Gamma_{(0,0,0)}$	0.0050	−0.1070	−0.3410
$\Gamma_{(90,0,0)}$	0.0230	−0.1072	−0.3510
$\Gamma_{(180,\ 0,\ 0)}$	0.0020	−0.1125	−0.3610
$\Gamma_{(270,\ 0,\ 0)}$	0.0240	−0.1160	−0.3600
$\Gamma_{(0,\ 90,\ 0)}$	−0.0010	−0.1009	−0.2690
$\Gamma_{(0,\ 180,\ 0)}$	0.0440	−0.0724	−0.3100
$\Gamma_{(0,\ 270,\ 0)}$	0.0350	0.0551	−0.2010
$\Gamma_{(0,\ 0,90)}$	0.0280	−0.0188	−0.2230
$\Gamma_{(0,\ 0,180)}$	0.0440	−0.0885	−0.2770
$\Gamma_{(0,0,270)}$	0.0030	−0.0594	−0.2860

on the other hand, has been the object of interest in the last years due to its accuracy in comparison with other schemes. It was shown that HPA leads to nonnegative condensed Fukui function indices that are more realistic.[38,39] It was also established that charges obtained from HPA predict more reliably trends of reactivity within a molecule in comparison to MPA,[34] natural bond orbital (NBO) analysis,[40−43] and methods based on the molecular electrostatic potential.[44] The stockholder character of HPA is the main cause of its advantages over other population analysis schemes.[45] Finally, it was also demonstrated that HPA has minimum loss of information when atoms are joined to form a molecule.[46−50] The intramolecular reactivity sequence of some chosen alkali halides was recently studied using HPA by Roy,[51] who has shown that the descriptors of local reactivity evaluated through this method correctly reproduce the strongest electrophilic center in all systems studied. Thus, in analyzing our results, we will pay more attention to the charges calculated through the Hirshfeld scheme, followed by ESP and MPA.

The population analysis for each AsA adsorbate is shown in Table 2. Hirshfeld charges are, in general, negative, except for the $\Gamma_{(0,270,0)}$ case, which has a slight positive charge (0.0551 e). The lowest-energy geometry $\Gamma_{(0,0,0)}$ is negatively charged with −0.1070 e. The largest amount of electron transfer is observed for the $\Gamma_{(270,0,0)}$ (−0.1160 e), followed by $\Gamma_{(180,0,0)}$ (−0.1125 e) and $\Gamma_{(90,0,0)}$ (−0.1072 e). All of these structures are qualitatively very similar to $\Gamma_{(0,0,0)}$, as was pointed out before. The other configurations have smaller electron transfers, probably due to the larger distance to the C_{60} molecule in comparison to that for the $\Gamma_{(0,0,0)}$-like structures. ESP population analyses have the same trend, being negative for all Γ geometries and with more intense charge transfers than that predicted through HPA. Mulliken charges, on the other side, are very small and positive, in general. The largest electron transfer is observed for $\Gamma_{(0,0,180)}$ (0.0440 e) and $\Gamma_{(0,180,0)}$ (0.0440 e). The trend of increasing charge with the increase of the AsA adsorbate proximity toward C_{60} is not perceived in MPA. Only the $\Gamma_{(0,90,0)}$ has a negative (and very small) electron transfer of −0.0010 e.

IV. Concluding Remarks

Many molecules noncovalently bound to carbon fullerenes and nanotubes have simple electric charge distributions, with a negative and/or a positive center, as in the case of amino acids, for example. In this case, the adsorption energy as a function of intermolecular distance has a single minimum related to a unique spatial configuration of the adsorbed molecule on the carbon nanostructure, and it is straightforward to calculate the binding energy. This is not the case of AsA, which has four −OH groups plus two oxygen atoms in a ring, all of them contributing to the AsA−C_{60} noncovalent bonding in several ways. In this system, the classical annealing simulation of a single AsA molecule interacting with C_{60} was found by us to be a very suitable method to obtain different initial geometries for studying AsA adsorption. This strategy could also predict the equilibrium structures for other complexes or molecules of interest with several negative and/or positive charged centers.

In this work, 10 lowest total energy geometries of AsA adsorbed on C_{60} were probed, the main structural features and charge transfer for each adsorbate being also determined. The lowest-energy configuration, $\Gamma_{(0,0,0)}$, corresponds to a geometry where two carbon atoms (denoted by C^1 and C^4) and two oxygen atoms (O^1 and O^6) are nearest to the C_{60} surface. This geometry results in a distance of 6.67 Å (7.23 Å) between the molecules' CMs according to the LDA (GGA) computations. The other optimized geometries have total energies very close to the value obtained for $\Gamma_{(0,0,0)}$, being larger by an average value of approximately 0.65 eV (0.45 eV) in the LDA (GGA). The adsorption energy (E_A) varies from −0.54 to −0.10 eV in the LDA data, and the sequence of configurations with increasing adsorption energy does not follow the corresponding sequence for increasing total energy. The adsorbate with the strongest interaction is also the closest to C_{60}. Adsorption energy as a function of the distance between the molecules CMs was plotted, showing characteristic curves of binding with a single minimum. Electron transfer was calculated using three different approaches, Mulliken, Hirshfeld, and ESP population analysis. The Hirshfeld scheme shows that the AsA molecule tends to be negatively charged (about −0.1 e for the lowest total energy adsorbates) for all configurations, except $\Gamma_{(0,270,0)}$. ESP charges are always negative and larger in magnitude, with an average value of approximately −0.3 e. There is a correlation between the distance between the molecules' CMs and the electron transfer for both methodologies, but no such correlation was observed when using Mulliken analysis, which also predicts very small and positive charges for all adsorbates.

A shortcoming of this work is that the calculations were performed only in vacuum. Water effects would probably decrease the strength of the AsA−C_{60} noncovalent interaction, and therefore, it is not certain that in the biological aqueous medium AsA should bind to C_{60}. A previous fullerene functionalization with NH_2, amide, or amine groups[52,53] could probably increase the binding energy of AsA with these decorated fullerenes. The demonstration of noncovalent AsA-functionalized C_{60} in biological media suggests that the administration of this complex should be more effective to prevent the oxidative damage and toxicity of C_{60}.[15] As a consequence, it is possible that the AsA−C_{60} associated with levodopa reduces the neurotoxicity generated by isolated levodopa.[16] In the latter case, new strategies for Parkinson's disease treatment by combining the clinical use of levodopa and potent antioxidants, that is, noncovalent AsA-functionalized C_{60}, should be envisaged. The results of this work come opportunely to stimulate further research in this direction, such as the development of chemical procedures for AsA−C_{60} noncovalent functionalization and the assessment of its oxidative damage and toxicity.

Acknowledgment. V.N.F. and B.S.C. are senior CNPq researchers and received financial support from CNPq-Rede NanoBioestruturas, Project N. 555183/2005-0. E.W.S.C. received financial support from CNPq-Process Number 304338/2007-9 and CNPq-Process Number 482051/2007-8. S.G.S. and F.F.M.J. were sponsored by a graduate fellowship from CNPq and CAPES, respectively. V.N.F. would like to acknowledge

Prof. D. Galvao, from UNICAMP, for the using of the DMOL3 and Forcite Plus codes.

References and Notes

(1) Kroto, H. W.; Heath, J. R.; O'Brien, S. C.; Curl, R. F.; Smalley, R. E. C_{60}: Buckminsterfullerene. *Nature* **1985**, *318*, 162–163.
(2) Kroto, H. W. C_{60}: Buckminsterfullerene, The Celestial Sphere that Fell to Earth. *Angew. Chem., Int. Ed. Engl.* **1992**, *31*, 111–129.
(3) Wudl, F. The Chemical Properties of Buckminsterfullerene (C_{60}) and the Birth and Infancy of Fulleroids. *Acc. Chem. Res.* **1992**, *25*, 157–161.
(4) Hirsch, A. *The Chemistry of the Fullerenes*; Thieme: Stuttgart, Germany, 1994.
(5) Bosi, S.; Da Ros, T.; Spalluto, G.; Prato, M. *Eur. J. Med. Chem.* **2003**, *38*, 913–923.
(6) Mroz, P.; Tegos, G. P.; Gali, H.; Wharton, T.; Sarna, T.; Hamblin, M. R. *Photochem. Photobiol. Sci.* **2007**, *6*, 1139.
(7) Colvin, V. *Nat. Biotechnol.* **2003**, *10*, 1166.
(8) Britz, D. A.; Khlobystov, A. N. *Chem. Soc. Rev.* **2006**, *35*, 637.
(9) Isakovic, A.; Markovic, Z.; Todorovic-Markovic, B.; Nikolic, N.; Vranjes-Djuric, S.; Mirkovic, M.; Dramicanin, M.; Harhaji, L.; Raicevic, N.; Nikolic, Z.; Trajkovic, V. *Toxicol. Sci.* **2006**, *91*, 173.
(10) Sayes, C. M.; Fortner, J. D.; Guo, W.; Lyon, D.; Boyd, A. M.; Ausman, K. D.; Tao, Y. J.; Sitharaman, B.; Wilson, L. J.; Hughes, J. B.; West, J. L.; Colvin, V. L. *Nano Lett.* **2004**, *4*, 1881.
(11) Tang, Y. J.; Ashcroft, J. M.; Chen, D.; Min, G.; Kim, C.-H.; Murkhejee, B.; Larabell, C.; Keasling, J. D.; Chen, F. F. *Nano Lett.* **2007**, *7*, 754.
(12) Woods, J. R., Jr.; Plessinger, M. A.; Miller, R. K. *Am. J. Obstet. Gynecol.* **2001**, *185*, 5.
(13) Castro, M.; Caprile, T.; Astuya, A.; Millan, C.; Reinicke, K.; Vera, J. C.; Vasquez, O.; Aguayo, L. G.; Nualart, F. *J. Neurochem.* **2001**, *78*, 815.
(14) Gershoff, S. N. *Nutr. Rev.* **1993**, *51*, 313.
(15) Sayes, C. M.; Gobin, A. M.; Ausman, K. D.; Mendez, J.; West, J. L.; Colvin, V. L. *Biomaterials* **2005**, *26*, 7587.
(16) Corona-Morales, A. A.; Castell, A.; Escobar, A.; Drucker-Colin, R.; Zhang, L. *J. Neurosci. Res.* **2002**, *71*, 121.
(17) Perdew, J. P.; Wang, Y. *Phys. Rev. B* **1992**, *45*, 13244.
(18) Perdew, J. P.; Burke, K.; Ernzerhof, M. *Phys. Rev. Lett.* **1996**, *77*, 3865.
(19) Wu, X.; Vargas, M. C.; Nayak, S.; Lotrich, V.; Scoles, G. *J. Chem. Phys.* **2001**, *115*, 8748.
(20) Milanesio, M.; Bianchi, R.; Ugliengo, P.; Roetti, C.; Viterbo, D. *J. Mol. Struct.: THEOCHEM* **1997**, *419*, 139.
(21) Mora, M. A.; Melendez, F. J. *J. Mol. Struct.: THEOCHEM* **1998**, *454*, 175.
(22) Juhasz, J. R.; Pisterzi, L. F.; Gasparro, D. M.; Almeida, D. R. P.; Csizmadia, I. G. *J. Mol. Struct.: THEOCHEM* **2003**, *401*, 666–667.
(23) Kónya, V. V.; Meszaros, P. G.; Viskolcz, B.; Csizmadia, I. G. *J. Mol. Struct.: THEOCHEM* **2003**, *397*, 666–667.
(24) (a) Delley, B. *J. Chem. Phys.* **1990**, *92*, 508. (b) Delley, B. *J. Chem. Phys.* **2000**, *113*, 7786.
(25) Dulak, M.; Wesolowski, T. A. *J. Mol. Model.* **2007**, *13*, 631.
(26) Furthmuller, J.; Hafner, J.; Kresse, G. *Phys. Rev. B* **1994**, *50*, 15606.
(27) Zhao, J.; Buldum, A.; Han, J.; Lu, J. P. *Nanotechnology* **2002**, *13*, 195.
(28) Chen, X. R.; Oshiyama, A.; Okada, S. *Phys. Rev. B* **2003**, *67*, 033408.
(29) Chen, X. R.; Oshiyama, A.; Okada, S. *Chem. Phys. Lett.* **2003**, *371*, 528.
(30) Saito, S.; Oshiyama, A. *Phys. Rev. Lett.* **1991**, *66*, 2637.
(31) Troullier, N.; Martins, J. L. *Phys. Rev. B* **1992**, *46*, 1754.
(32) Chen, X.-R.; Bai, Y.-L.; Zhu, J.; Yang, X.-D. *Phys. Rev. A* **2004**, *69*, 034701.
(33) Inada, Y.; Orita, H. *J. Comput. Chem.* **2008**, *29*, 225.
(34) Mulliken, R. S. *J. Chem. Phys.* **1955**, *23*, 1833.
(35) Hirshfeld, F. L. *Theor. Chim. Acta* **1977**, *44*, 129.
(36) Singh, C. U.; Kollman, P. A. *J. Comput. Chem.* **1984**, *5*, 129.
(37) Roy, R. K.; Hirao, K.; Krishnamurty, S.; Pal, S. *J. Chem. Phys.* **2001**, *115*, 2901.
(38) Roy, R. K.; Pal, S.; Hirao, K. J. *J. Chem. Phys.* **1999**, *110*, 8236.
(39) Parr, R. G.; Yang, W. J. *J. Am. Chem. Soc.* **1984**, *106*, 4049.
(40) Foster, J. P.; Weinhold, F. *J. Am. Chem. Soc.* **1980**, *102*, 7211.
(41) Rives, A. B.; Weinhold, F. *Int. J. Quantum Chem. Symp.* **1980**, *14*, 201.
(42) Reed, A. E.; Weinhold, F. *J. Chem. Phys.* **1983**, *78*, 4066.
(43) Reed, A. E.; Weinstock, R. B.; Weinhold, F. *J. Chem. Phys.* **1985**, *83*, 735.
(44) Bonaccorsi, R.; Scrocco, E.; Tomasi, J. *J. Chem. Phys.* **1970**, *52*, 5270.
(45) Roy, R. K.; Hirao, K.; Pal, S. *J. Chem. Phys.* **2000**, *113*, 1372.
(46) Parr, R. G.; Nalewajski, R. F. *Proc. Natl. Acad. Sci. U.S.A.* **2000**, *97*, 8879.
(47) Nalewajski, R. F. *Phys. Chem. Chem. Phys.* **2002**, *4*, 1710.
(48) Ayers, P. W. *J. Chem. Phys.* **2000**, *113*, 10886.
(49) Ayers, P. W. *Proc. Natl. Acad. Sci. U.S.A.* **2000**, *97*, 1959.
(50) Ayers, P. W.; Morisson, R. C.; Roy, R. K. *J. Chem. Phys.* **2002**, *116*, 8731.
(51) Roy, R. K. *J. Phys. Chem. A* **2003**, *107*, 10428.
(52) Zanella, I.; Lemos, V.; Filho, J. M.; Guerini, S. *J. Comput. Theor. Nanosci.* **2008**, *5*, 1.
(53) Ramanathan, T.; Fisher, F. T.; Ruoff, R. S.; Brinson, L. C. *Chem. Mater.* **2005**, *17*, 1290–1295.

JP8048263